Distributed Multi-User MIMO Transmission Using Real-Time Sigma-Delta-Over-Fiber for Next Generation Fronthaul Interface

Chia-Yi Wu, Haolin Li, Olivier Caytan, Joris Van Kerrebrouck, Laurens Breyne, Johan Bauwelinck, *Senior Member, IEEE*, Piet Demeester, *Fellow, IEEE*, and Guy Torfs, *Senior Member, IEEE*

***Abstract*—To achieve the massive device connectivity and high data rate demanded by 5G, wireless transmission with wider signal bandwidths and higher-order multiple-input multiple-output (MIMO) is inevitable. This work demonstrates a possible function split option for the next generation fronthaul interface (NGFI). The proof-of-concept downlink architecture consists of real-time sigma-delta modulated signal over fiber (SDoF) links in combination with distributed multi-user (MU) MIMO transmission. The setup is fully implemented using off-the-shelf and in-house developed components. A single SDoF link achieves an error vector magnitude (EVM) of 3.14% for a 163.84 MHz-bandwidth 256-QAM OFDM signal (958.64 Mbps) with a carrier frequency around 3.5 GHz transmitted over 100 m OM4 multi-mode fiber at 850 nm using a commercial QSFP module. The centralized architecture of the proposed setup introduces no frequency asynchronism among remote radio units. For most cases, the 2 × 2 MU-MIMO transmission has little performance degradation compared to SISO, 0.8 dB EVM degradation for 40.96 MHz-bandwidth signals and 1.4 dB for 163.84 MHz-bandwidth on average, implying that the wireless spectral efficiency almost doubles by exploiting spatial multiplexing. A 1.4 Gbps data rate (720 Mbps per user, 163.84 MHz-bandwidth, 64-QAM) is reached with an average EVM of 6.66%. The performance shows that this approach is feasible for the high-capacity hot-spot scenario.**

***Index Terms*—Distributed antenna system, multi-user multiple-input multiple-output, next generation fronthaul interface, radio-over-fiber, sigma-delta modulation.**

Manuscript received July 19, 2019; revised August 28, 2019 and October 11, 2019; accepted October 11, 2019. Date of publication October 16, 2019; date of current version February 12, 2020. This work was supported in part by the ERC Advanced Grant ATTO Project (695495) and in part by the H2020 5G-PHOS Project (761989). *(Corresponding author: Chia-Yi Wu.)*

C.-Y.Wu, H. Li, O. Caytan, J. Van Kerrebrouck, J. Bauwelinck, P. Demeester, and G. Torfs are with IDLab, Department of Information Technology, Ghent University–imec, 9052 Ghent, Belgium (e-mail: chiayi.wu@ugent.be; haolin.li@ugent.be; olivier.caytan@ugent.be; joris.vankerrebrouck@ugent.be; johan.bauwelinck@ugent.be; piet.demeester@ugent.be; guy.torfs@ugent.be).

L. Breyne is with IDLab, Department of Information Technology, Ghent University–imec, 9052 Ghent, Belgium, and also with the Photonics Research Group, Department of Information Technology, Ghent University–imec, 9052 Ghent, Belgium (e-mail: laurens.breyne@ugent.be).

Color versions of one or more of the figures in this article are available online at http://ieeexplore.ieee.org.

Digital Object Identifier 10.1109/JLT.2019.2947786

I. Introduction

TO MEET the highly challenging demands of 5G—massive device connectivity and high data rate—wider signal bandwidths, increased base station density and higher-order multiple-input multiple-output (MIMO) technologies are expected [1]. The radio access network (RAN) must evolve to accommodate the 5G data traffic.

In the 4G era, the centralized RAN (C-RAN) architecture has demonstrated its advantages: lower deployment cost, easier maintenance, and higher power efficiency [2]. By aggregating several baseband units (BBUs) at a central unit (CU) and connecting the CU to remote radio units (RRUs) using radio-over-fiber (RoF) technologies, the C-RAN architecture also eases the latency requirement and the backhaul traffic congestion while coordinating several RRUs to operate like a distributed MIMO system, also often referred to as coordinated multi-point (CoMP) [3], via only the fronthaul network [4].

5G C-RAN with the next generation fronthaul interface (NGFI) has been proposed by China Mobile Research Institute [5]. An extra layer, distributed unit (DU), is introduced. A CU is connected to several DUs via the midhaul network; each DU serves several RRUs via the fronthaul network. 3GPP has decided to split the CU and DU between the packet data convergence protocol (PDCP) and radio link control (RLC) layer, as shown in Fig. 1; the split between DU and RRU is still open for discussions [2], [6].

Radio-over-fiber (RoF) technologies are among the most convincing candidates for the fronthaul network, i.e. the DU-RRU interface (Fig. 1), because of their high capacity and low latency [7]. There are three main RoF schemes (Fig. 2): digitized radio-over-fiber (DRoF), analog radio-over-fiber (ARoF) and sigma-delta modulated signal over fiber (SDoF).

For DRoF, common public radio interface (CPRI) [8] and enhanced CPRI (eCPRI) [9] can be applied to split option 8 and intra-physical (intra-PHY) layer split options [6] respectively. Generally, the improved optical bit-rate efficiency of intra-PHY layer splits, compared to option 8, comes with the cost of more complicated RRUs. For ARoF and SDoF, split option 9 is first introduced by [10]. It keeps the higher part of the radio frequency (RF) processing (high-RF layer), e.g. up-conversion, at DUs and leaves only the lower part of the RF processing (low-RF layer), including amplifiers and filters, at RRUs. Option 9 significantly

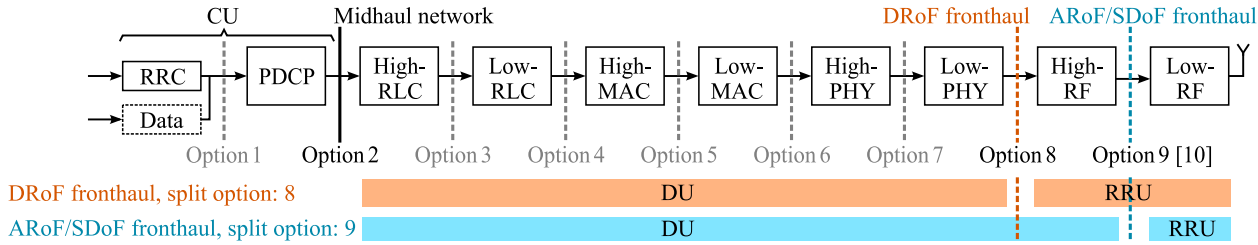

Fig. 1. Function split options [2] while applying digitized radio-over-fiber (DRoF), analog radio-over-fiber (ARoF) and sigma-delta modulated signal over fiber (SDoF) to the fronthaul network. (CU: central unit; DU: distributed unit; RRU: remote radio unit. RRC: radio resource control; PDCP: packet data convergence protocol layer; RLC: radio link control layer; MAC: medium access control layer; PHY: physical layer; RF: radio frequency layer.)

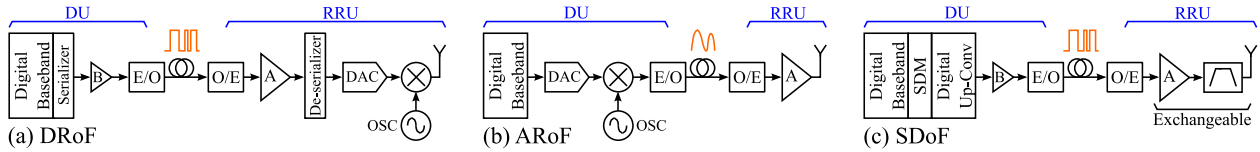

Fig. 2. (a) Digitized radio-over-fiber (DRoF), (b) analog radio-over-fiber (ARoF) and (c) sigma-delta modulated signal over fiber (SDoF) link. (E/O: electrical-to-optical; O/E: optical-to-electrical; B: binary driver; A: amplifier; DAC: digital-to-analog converter; OSC: oscillator; SDM: sigma delta modulator.)

decreases the RRU complexity. However, it does not guarantee a better optical bit-rate efficiency. When applying SDoF for option 9, both this work and [10] up-convert the signals digitally to the desired carrier frequency at the DU using the architecture proposed in [11]. The bit rate over fiber is consequently equal to four times the desired carrier frequency. [10] uses a 960 MHz carrier frequency and achieves a bit-rate efficiency gain of 1.85 with respect to CPRI. This work has a lower bit-rate efficiency (0.43 with respect to CPRI) because the signals are up-converted to 3.5 GHz.

In our previous works [12]–[14], we have discussed the differences between the three main RoF schemes. SDoF combines the advantages of DRoF and ARoF. Like the widely-used DRoF, the requirements on analog devices are significantly relaxed compared to ARoF and it is possible to use non-linear optical transmitters. The simple, inexpensive and power-efficient RRU architecture as shown in Fig. 2c makes SDoF more scalable in terms of the RRU density compared to DRoF. Furthermore, it will be shown in the measurement results that SDoF has also high scalability for different signal bandwidths without modifying the underlying hardware. We have published the superior performance of transmitting single carrier data over SDoF links in real-time for the sub-6 GHz [14] and 22.75-27.5 GHz band [15]. This work focuses on the benefits of combining SDoF links and a distributed MIMO system.

For both ARoF and SDoF, because the up-converters are co-located at the DU, the carrier synchronization between transmitters—one of the large challenges for distributed MIMO transmission [16]—is no longer a problem. The distributed MIMO SDoF system suffers no performance degradation caused by the frequency asynchronism between transmitters, thus needs no sophisticated synchronization algorithm.

Several recently published papers present the performance of MIMO ARoF systems [17]–[19]. In [20], offline-generated sigma-delta modulated signals are used to demonstrate the performance of a single-carrier MIMO SDoF system.

This paper presents a real-time FPGA-based 2×2 distributed multi-user MIMO (MU-MIMO) orthogonal frequency division multiplexing (OFDM) transmission using SDoF links targeting 5G NGFI downlink. The demonstration, implemented using off-the-shelf and in-house developed components, extends our SDoF links for the sub-6 GHz band [14] with distributed MIMO transmission. This work shows that, while guaranteeing the carrier frequency synchronism for distributed MIMO transmission, SDoF can have low deployment cost owing to its relaxed device requirements compared to ARoF and simple RRU architecture compared to DRoF. The demonstrated architecture, using a commercial QSFP-100G-SR4 and multi-mode fibers (MMFs), is a possible solution for the fronthaul network deployment for the high-capacity hot-spot scenario of the 5G enhanced mobile broadband (eMBB) service [21]. The setup has also been accepted as a demo session for the 45th European Conference on Optical Communication [22].

Section II introduces the system architecture and experimental methodology, including the detailed measurement setup, measurement workflow, and applied algorithms. In Section III, the SDoF link performance over different OFDM signal bandwidths is provided, followed by the MIMO measurement results and the performance evaluation of the carrier frequency asynchronism among RRUs. Section IV concludes the paper.

II. System Architecture and Experimental Methodology

Fig. 3 shows a 2×2 MU-MIMO downlink transmission using SDoF links. Split option 9 in Fig. 1, which places the fronthaul interface between the high and low RF layer, is chosen for this architecture. The system consists of one distributed

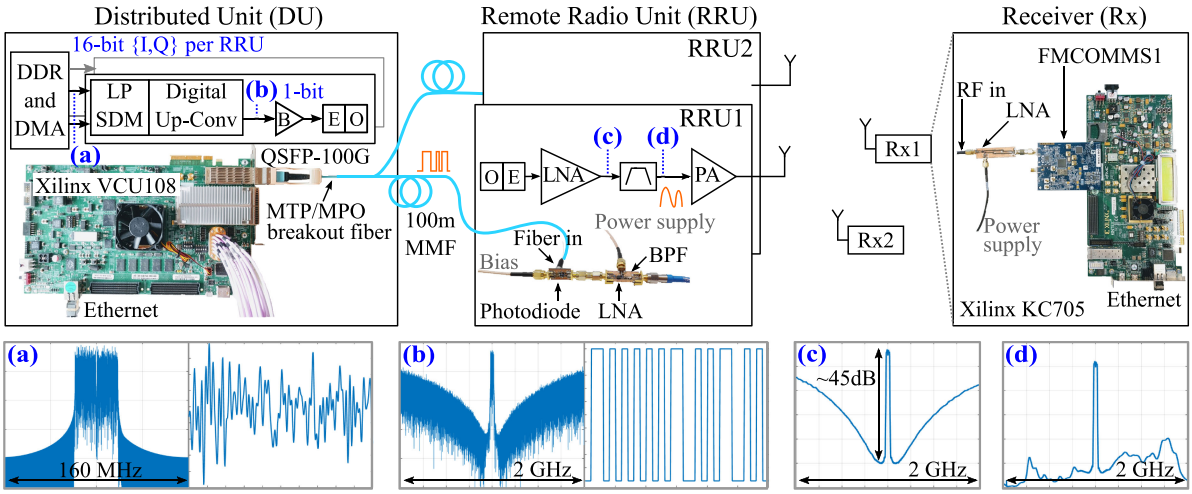

Fig. 3. System architecture. (DMA: direct memory access; LP SDM: low-pass sigma-delta modulator; B: binary driver; E-O: electrical-to-optical; O-E: optical-to-electrical; LNA: low-noise amplifier; BPF: band-pass filter; PA: power amplifier.) (a) Spectrum and waveform of a 40.96 MHz OFDM baseband signal generated by MATLAB; (b) simulated spectrum and waveform of the digital up-conversion output; (c) measured spectrum of the non-return-to-zero (NRZ) output signal of the LNA; (d) measured spectrum of the BPF output.

TABLE I
OFDM SIGNAL PARAMETERS

Parameters	Values			
Carrier frequency	3.44064 GHz			
Cyclic prefix (CP) size	1/4			
Bandwidth (MHz)	20.48	40.96	81.92	163.84
N_{FFT}	64	128	256	512
N_{DC} + N_{Null}	8	14	14	28
N_{Pilots}	4	6	8	16
Data rate per user				
64-QAM (Mbps)	79.87	165.89	359.42	718.85
256-QAM (Mbps)	106.50	221.18	479.23	958.46

N_{FFT}: number of subcarriers (FFT/IFFT size);
N_{DC} / N_{Null} / N_{Pilots}: number of DC/null/pilot subcarriers.

unit (DU), two remote radio units (RRUs) and two independent receivers/users. The implemented DU includes two parts: the low physical (PHY) and high-RF layer. MATLAB scripts are used for the low PHY processing, e.g. the OFDM signal generation and MIMO precoding. The processing of the high-RF layer—sigma-delta modulation and up-conversion—is real-time implemented on the FPGA. Only the band-pass filters (BPFs) and amplifiers are placed at the RRUs.

A. MU-MIMO OFDM Signal

MIMO technologies have been widely used to increase the spectral efficiency of wireless communication systems or the reliability of the received signals [23]. MU-MIMO transmission multiplies the transmitted data rate by exploiting spatial multiplexing; independent users receive different data sequences simultaneously while using the same wireless frequency band.

The OFDM signal parameters used in the demonstration are summarized in Table I. For the ease of implementation and using the a priori knowledge that the experiments will be carried out in an indoor environment, the parameters are based on the IEEE 802.11ac specifications [24]. The DC, null and pilot subcarrier indices follow the specification. However, it should be noted that the SDoF approach is standard agnostic, hence the employed modulation format can be easily adapted. The signal bandwidth is adjusted to fit the available sampling rates of the analog-to-digital converters at the receivers.

The received baseband data on a subcarrier can be written as

$$\begin{bmatrix} R_1 \\ R_2 \end{bmatrix} = \underbrace{\begin{bmatrix} H_{11} & H_{21} \\ H_{12} & H_{22} \end{bmatrix}}_{\text{Channel matrix: } \mathbf{H}} \begin{bmatrix} X_1 \\ X_2 \end{bmatrix} + \begin{bmatrix} W_1 \\ W_2 \end{bmatrix} \quad (1)$$

where all elements in (1) are complex number; R_j is the signal received by receiver j; H_{ij} denotes the equivalent channel frequency response (CFR) in baseband between RRU i and receiver j; X_i is the baseband data transmitted by RRU i; W_j is the additive noise.

The workflow has two phases as shown in Fig. 4: the training and data transmission phase.

1) Training Phase: During the training phase, frequency-interleaved training sequences for channel estimation, illustrated in Fig. 4, are transmitted; for each subcarrier, within one given OFDM frame, either RRU 1 or RRU 2 transmits QPSK data while the other one transmits nothing. The least square channel estimation [25] is applied to estimate the CFRs. For the case with two transmitters, the training sequences should last at least two OFDM frames. In a noisy environment, using longer training sequences, i.e. averaging over multiple estimated H_{ij}, results in better channel estimation results.

2) Data Transmission Phase: During the data transmission phase, for each subcarrier, the precoded data is transmitted. The

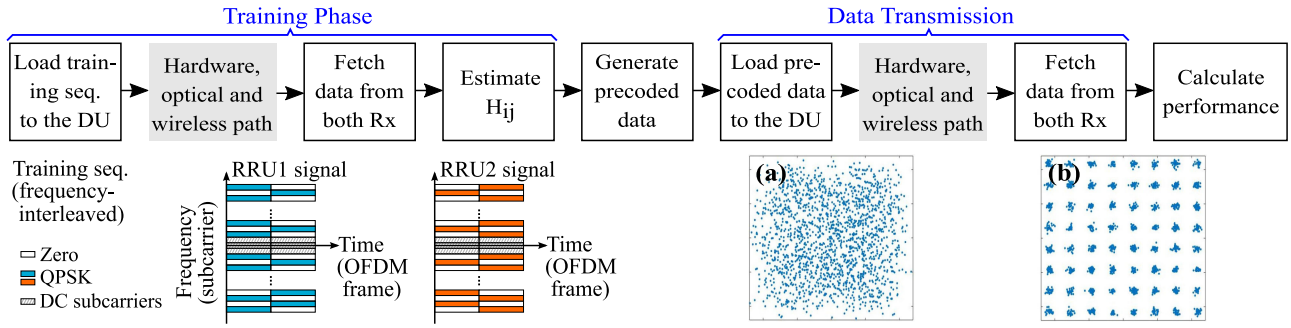

Fig. 4. Measurement workflow and the illustration of frequency-interleaved training sequences. (a) An example of the constellation diagram of precoded data; (b) an example of the constellation diagram of received data.

precoded data is generated based on the zero-forcing technique.

$$\begin{bmatrix} X_1 \\ X_2 \end{bmatrix} = \underbrace{\begin{bmatrix} \alpha & -\beta\frac{\hat{H}_{21}\hat{H}_{11}^*}{\hat{H}_{11}^*\hat{H}_{11}} \\ -\alpha\frac{\hat{H}_{12}\hat{H}_{22}^*}{\hat{H}_{22}^*\hat{H}_{22}} & \beta \end{bmatrix}}_{\text{Precoding matrix: } \mathbf{G}} \begin{bmatrix} S_1 \\ S_2 \end{bmatrix} \tag{2}$$

where $\hat{H}_{ij}$ denotes the estimated CFR between RRU i and receiver j during the latest training phase and S_i is the baseband data expected to be received by receiver i; α and β are two real constants that have the same values for all subcarriers in an OFDM frame.

The precoding matrix **G** in (2) is applied, instead of the inverse of the channel matrix **H** in (1), because it is easier to adjust the dynamic range of the precoded data to fit the input range of SDMs by tuning the two constants α and β.

Assuming the channel estimation is sufficiently accurate, i.e. $\hat{H}_{ij} \approx H_{ij}$. The received baseband data (1) can be written as

$$\begin{bmatrix} R_1 \\ R_2 \end{bmatrix} = \begin{bmatrix} c_1 & 0 \\ 0 & c2 \end{bmatrix} \begin{bmatrix} S_1 \\ S_2 \end{bmatrix} + \begin{bmatrix} W_1 \\ W_2 \end{bmatrix} \tag{3}$$

where

$$c_1 = \alpha\left(H_{11} - H_{21}\frac{H_{12}H_{22}^*}{H_{22}^*H_{22}}\right) \tag{4}$$

and

$$c_2 = \beta\left(H_{22} - H_{12}\frac{H_{12}H_{22}^*}{H_{22}^*H_{22}}\right) \tag{5}$$

Ideally, a receiver i shall receive its data S_i without interference ($S_{j,j\neq i}$) as shown in Fig. 4b. From the measurement results, it will become clear that the performance difference between the MU-MIMO setup and a single-input single-output (SISO) link is relatively small in terms of error vector magnitude (EVM).

B. Sigma-Delta Modulated Signal Over Fiber

1) Distributed Unit (DU): The DU, including the SDMs and digital up-conversion, is implemented on a *Xilinx Virtex Ultrascale* FPGA (VCU108). The MATLAB-generated OFDM baseband signals with bandwidths up to 163.84 MHz as indicated in Table I, whose in-phase (I) and quadrature (Q) signal are both 16-bit, are loaded to the DDR on the DU via the Ethernet connection, streamed to 2 × 2 (one I-Q pair per RRU) low-pass SDMs using a *Xilinx* AXI direct memory access (DMA) IP, and then modulated at 7 GSps (sample per second).

To have a high signal-to-noise and distortion ratio, second-order low-pass SDMs are chosen for this architecture. A parallel multi-stage scheme is employed to achieve the desired sample rate. The quantization noise is shaped by the low-pass SDMs to higher frequencies. The detailed hardware implementation of the SDM can be found in our previous work [26]. Digital up-conversion [11] translates the modulated I and Q signal (both 1-bit) to one 14 Gbps binary signal with a center frequency around 3.5 GHz for each RRU.

The bit-rate efficiency, calculated by dividing the transmitted data bandwidth by the bit rate over fiber, is 11.7 MHz/Gbps. Using the example in [8], the bit-rate efficiency of CPRI is 27.12 MHz/Gbps. The high bit rate, resulting in the relatively low optical bit-rate efficiency, is required to perform digital up-conversion at the DU and comes with the benefit of a simple RRU architecture.

Fig. 3a shows the spectrum and waveform of the generated signal. Fig. 3b shows the simulated spectrum and waveform after sigma-delta modulation and digital up-conversion using MATLAB with fixed-point representation; it can be seen that the quantization noise is pushed out of the band of interest.

Each non-return-to-zero (NRZ) signal is converted to the optical domain using a QSFP-100G-SR4 module and transmitted over an OM4 MMF. The QSFP-100G-SR4 module has four 850 nm VCSELs (vertical-cavity surface-emitting lasers); we use only two of them to drive two MMFs. Each MMF connects the DU to one RRU. The QSFP module supports link lengths up to 100 m for OM4 MMFs. The maximum optical launch power per lane is approximately 2.4 dBm. Note that the optical link lengths can be largely extended if single-mode QSFP modules and fibers are exploited [14].

2) Remote Radio Unit (RRU): At each RRU, the received optical signal is converted back to the electrical domain using a GaAs PIN photodiode with a responsivity around 0.4 A/W; the photodiode is impedance-matched to the low-noise amplifier (LNA), *Mini-Circuits* PMA3-83LN+, to maximize the power transfer at 3.5 GHz [27]. The LNA amplifies the electrical signal coming from the photodiode; it has a low noise figure of 1.3 dB

and 20.8 dB gain when operating at 5V supply. The measured spectrum at the output of an LNA is shown in Fig. 3c; a spectrum similar to Fig. 3b is observed.

Then, the out-of-band quantization noise is filtered by a BPF as shown in the measured spectrum Fig. 3d. The filtered analog signals are amplified by power amplifiers (PAs), followed by in-house developed air-filled substrate-integrated-waveguide (AFSIW) cavity-backed slot antennas (Fig. 3b in [28]) to transmit the radio-frequency (RF) signals. *Mini-Circuits* amplifiers ZX60-83LN-S+ are used as the PAs. The power measured at the PA output is -2.51 dBm/40.96 MHz (-2.70 dBm/163.84 MHz). The antennas are matched to a 50 Ω impedance between 2.95 GHz to 3.90 GHz. Note that the position of the PA and BPF are exchangeable if using a switching-mode power amplifier [10], [20].

C. Receiver and Signal Processing

The two receivers, each with an architecture identical to a SISO receiver, operate independently. They use the same antennas as the RRUs. For each receiver, the antenna is first connected to an LNA. The amplified received signal is down-converted using a zero intermediate frequency (zero-IF) receiver and sampled by an analog front-end evaluation kit (*Analog Device FMCOMMS1-EBZ*) at 327.68 MHz ($2\times$ the largest signal bandwidth listed in Table I). A *Xilinx Kintex 7* FPGA (KC705) collects the data for offline signal processing using MATLAB.

The signal processing includes OFDM frame boundary detection, carrier frequency offset (CFO) correction using the algorithm proposed in [29], fast Fourier transform (FFT), least-square channel estimation and QAM demodulation.

The demonstration workflow as illustrated in Fig. 4 is fully realized in MATLAB. As mentioned in Subsection II-A, the workflow includes two parts: the training phase and data transmission. The CFRs are estimated during the training phase. An ideal channel information feedback is assumed. The estimated CFRs are used to generate precoded data (2). Then, the data transmission starts with loading the precoded data to the DU. At the receivers, after canceling the effect of the channel and the CFO, the received data is demodulated. The performance is presented with the EVM values.

III. Measurement Results

In this section, the transmitter performance is provided by transmitting wide-bandwidth OFDM signals over an SDoF link. The distributed MIMO performance is measured in a typical office environment; the SISO performance is provided as a baseline. In the end, to highlight the advantage of using SDoF links for distributed MIMO deployment, we also evaluated the performance degradation by deliberately introducing frequency asynchronism between RRUs, as would be expected when up-conversion is performed at the RRU, e.g. 4G C-RAN [30]. The performance is presented in root-mean-square error vector magnitude (EVM) normalized to the average constellation power.

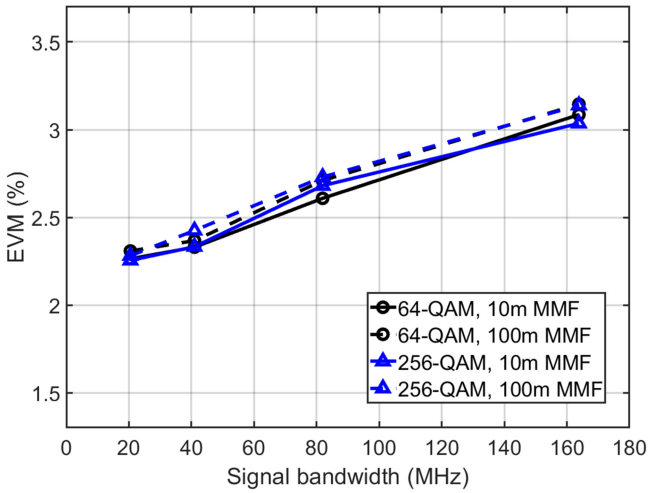

Fig. 5. Measured EVM vs. signal bandwidth.

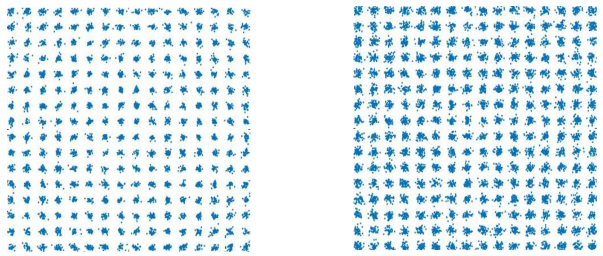

(a) 20.48MHz-bandwidth, 100m MMF EVM: 2.28% (-32.84 dB)

(b) 163.84MHz-bandwidth, 100m MMF EVM: 3.14% (-30.06 dB)

Fig. 6. Constellation diagrams of the OFDM signals transmitted over 100 m multi-mode fiber (MMF).

A. Sigma-Delta Modulated OFDM Signals Over Fiber

To show the quality of the SDoF link, the performance is measured without the wireless path. The output of the power amplifier is directly connected to an *Analog Device* FMCOMMS1-EBZ; appropriate attenuation is applied in between to prevent the receiver chain from saturation. The same reference clock is provided for the up-conversion and down-conversion, i.e. there is no CFO. Fig. 5 shows the EVM values versus different signal bandwidths and Fig. 6 shows the received constellation diagrams.

There is no significant performance difference in terms of EVM between the 64-QAM and 256-QAM cases. The performance degrades as the signal bandwidth increases because of two reasons: First, the total transmitted signal power is kept the same; thus, when the signal bandwidth increases, the power spectrum density (PSD) of the signal decreases while the noise PSD stays the same. Second, the oversampling ratio (OSR)

$$OSR = \frac{f_{\Sigma\Delta}/2}{BW} \tag{6}$$

decreases resulting in the increase of noise PSD; $f_{\Sigma\Delta}$ is the sampling rate of the SDM and BW is the signal bandwidth. The EVM values are higher when transmitting over a 100 m MMF. Nevertheless, the 3.14% EVM of the 163.84 MHz-bandwidth

OFDM signal transmitted over a 100 m MMF is lower than the 3GPP TS 36.104 EVM requirements: 3.5% (−29.12 dB) for 256-QAM [31].

The identical hardware architecture is used for all measured bandwidths, implying the high scalability of the SDoF link. The optical bit-rate efficiency is not considered as a severe issue in this work because each DU-RRU link uses one fiber in this demonstration. For network architectures that require higher bit-rate efficiency, transmitting baseband signals over fiber and performing up-conversion at RRUs can largely decrease the line rate. However, the RRU complexity will increase.

It is possible to reach longer link lengths by exploiting QSFP modules for single-mode fibers. As presented in our previous work [14], the SDoF link performance is sufficient up to 20 km single-mode fibers.

B. Distributed MIMO

The combined optical-wireless performance is measured in an office that is 8 m long, 4.5 m wide and 3.5 m tall approximately, with a 100 m MMF between the DU and each RRU. Fig. 7 shows the photo and simplified layout of the room and the measured EVM values. The furniture in the room, especially the metallic surfaces of the heater and shelves, forms a multipath-rich environment.

The directions of the RRU antennas are illustrated in the figure. The receiver antennas always face the nearest RRU antenna. Without loss of generality, the receiver (Rx) that is geometrically closer to RRU 1 is named Rx 1, denoted with the filled icons; the hollowed icons represent Rx 2. The total transmit power was kept the same for the SISO and MIMO cases. No common reference clock is provided to the DU and receivers. Since the up-conversion is performed at the DU, there is no carrier frequency asynchronism between the two RRUs. The CFO between the RRUs and receivers is estimated and compensated offline using MATLAB.

We measured 64-QAM OFDM signals with two different signal bandwidths: 40.96 MHz (Fig. 7a) and 163.84 MHz (Fig. 7b). For 40.96 MHz MIMO cases, the average EVM of all cases and two receivers is 3.53% (−29.04 dB). It is possible to transmit 256-QAM signals; however, to make a fair comparison with 163.84 MHz cases, 64-QAM is chosen. The average performance degradation compared to the SISO transmission (3.22%, −29.83 dB) is 0.8 dB. The average EVM for 163.84 MHz MIMO cases is 6.66% (−23.52 dB) and 5.66% (−24.94 dB) for SISO; the average performance degradation is 1.42 dB.

The MIMO transmission has the best performance when the signals from both RRUs are strong enough to estimate H_{ij} accurately and when each receiver is close to one RRU. Fig. 8 a shows the magnitude of H_{ij} of the case with the best performance: case 1 in Fig. 7. The magnitude values are calculated using the signed 16-bit I and Q values collected by *Analog Device* FMCOMMS1-EBZ without any normalization. During the MIMO transmission, the desired data signal for Rx 1 comes from RRU 1 and the interference comes from RRU 2. As shown in Fig. 8a, the magnitude of the signal CFRs, H_{11} and H_{22}, are both sufficiently larger than the magnitude of the interference

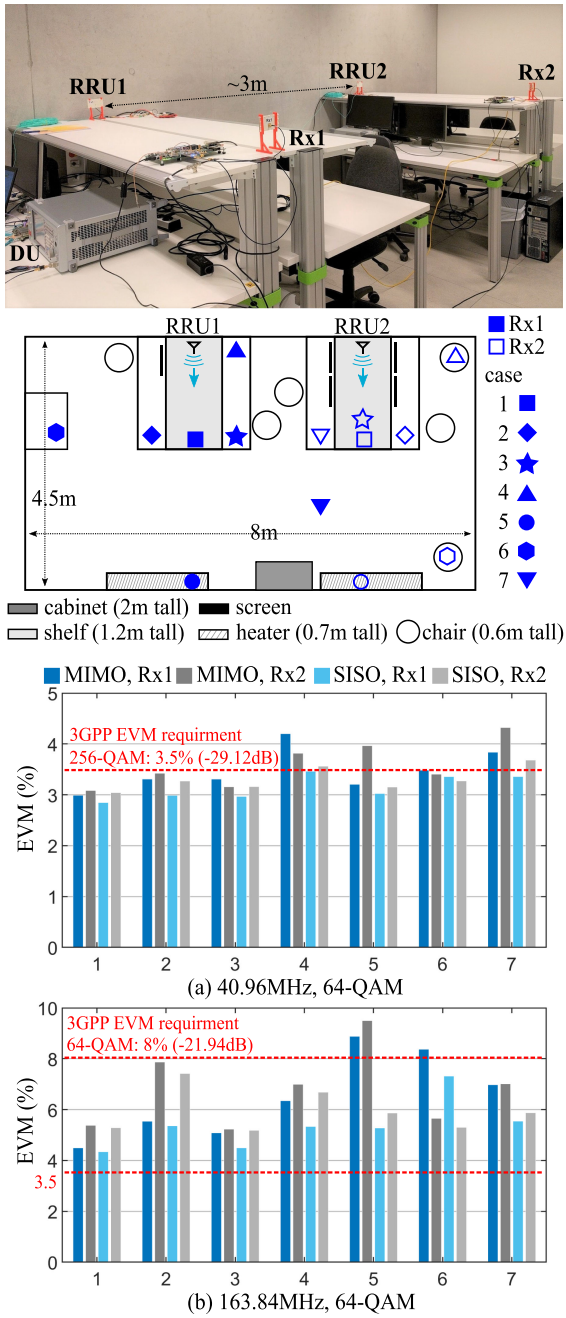

Fig. 7. Measurement setup, simplified layout of the room and the distributed MIMO performance of two bandwidths: (a) 40.96 MHz; (b) 163.84 MHz.

CFRs, H_{12} and H_{21}. Therefore, there is little performance degradation between the MIMO and SISO transmission. Case 5 has a similar setup geometry setup but with longer distances. The interference is strong compared to the signal as shown in Fig. 8b. Almost 4 dB EVM value degradation is measured between the MIMO and SISO transmission. Note that the performance can be improved using stronger power amplifiers.

More details about the CFRs for each case can be found in the appendix. The MIMO channels are analyzed using the singular values of channel matrices (**H**).

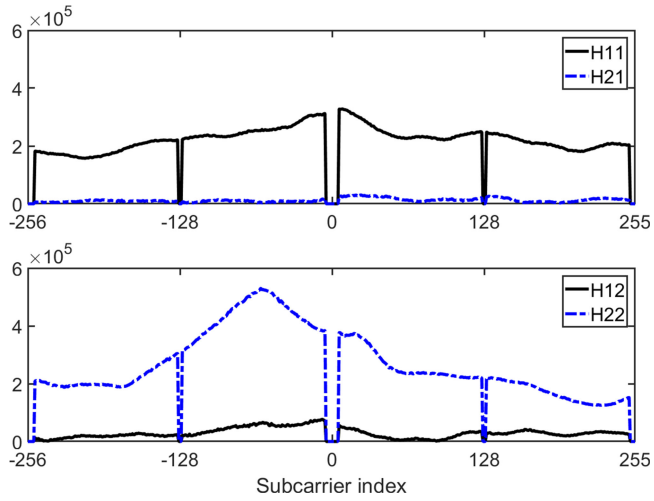

(a) Case 1 (Fig. 7), 163.84 MHz

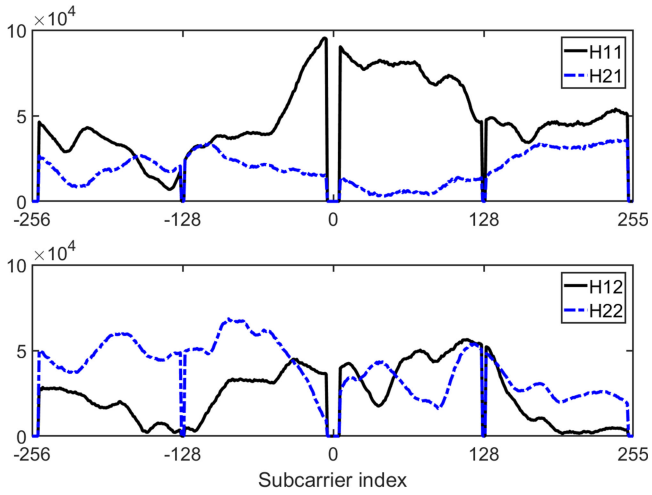

(b) Case 5 (Fig. 7), 163.84 MHz

Fig. 8. Magnitude of the estimated channel frequency responses (H_{ij}).

In general, the MIMO performance is comparable to the SISO transmission, implying that the wireless spectral efficiency significantly increases by exploiting spatial diversity.

C. Impact of Frequency Synchronization Error

This subsection highlights one of the benefits of the proposed architecture by measuring the EVM values versus carrier frequency differences between RRUs. The impact of frequency asynchronism for 4G C-RAN has been evaluated in [30] with simulation results. For different base station classes, a carrier frequency error ranging from ± 0.05 to ± 0.25 ppm, ± 175 Hz to ± 875 Hz for 3.5 GHz, is allowed (3GPP TS 36.104 [31] for E-UTRA and 3GPP TS 38.104 [32] for 5G New Radio (NR) base station). Algorithms have been developed to estimate and compensate the multiple carrier frequency offsets for CoMP transmissions [33]. Both the estimation and compensation are challenging and require complex computation.

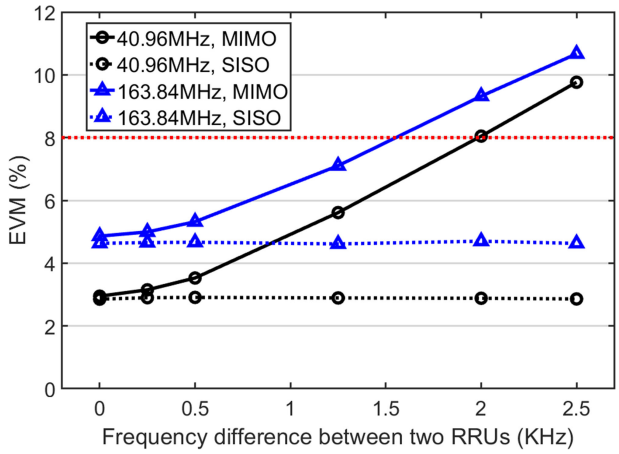

Fig. 9. Measured EVM vs. carrier frequency offset between two remote radio units (RRUs).

Owing to this centralized architecture, the distributed MIMO system with SDoF links has no frequency synchronization error. The carrier frequencies of the two RRUs are always synchronous, i.e. the CFO between a receiver and every RRU is the same. To evaluate the impact of frequency synchronization error, extra CFO is added to RRU 2.

The CFO effect can be modeled as a phase shift growing linearly with the time index [34]. Neglecting the effect of the multipath channel and noise, the received and sampled time-domain baseband signal can be written as

$$r[n] = x[n]e^{j2\pi \frac{\Delta f}{f_s} n} \tag{7}$$

where $x[n]$ and $r[n]$ are the transmitted and received baseband signal in the time domain, the integer n is the time index, Δf is the CFO in Hz and f_s is the OFDM sampling frequency. Extra CFO is added by rotating each sample of the time domain sequence $x[n]$ with the phase $2\pi(\Delta f/f_s)n$ while generating the 64-QAM OFDM signals using MATLAB.

The receivers are placed as the case 1 in Fig. 7 that has strong line-of-sight paths between both RRUs and receivers. The averaged EVM values (over Rx 1 and Rx 2) are shown in Fig. 9. When there is no frequency difference between the two RRUs, the MIMO performance is almost as good as SISO; the EVM difference is about 0.3 dB. However, even with a difference as small as 250 Hz, performance degradation is noticeable; the EVM difference between the MIMO and SISO transmission increases to 0.7 dB. The performance gap between the MIMO and SISO case grows rapidly when the carrier frequency difference increases.

The proposed architecture up-converts the sigma-delta modulated signals to 3.5 GHz at one DU and transmits the RF signals to the RRUs over fiber. Up-converting both signals at one DU makes it possible to use the same local oscillator signal, thus guarantees the carrier synchronism between the two RRUs. DRoF-based C-RAN, in contrast to the proposed architecture, generates the carrier signals at each RRU separately. As frequency inaccuracy can be introduced while generating each

carrier signal [35], its performance may consequently degrade due to carrier frequency asynchronism between RRUs.

With the ambition to increase the number of RRUs, to compensate multiple CFOs will become not feasible. Hence, an architecture that can guarantee the frequency synchronization between RRUs—as we proposed—is highly beneficial.

IV. Conclusion

We have demonstrated a fully implemented 2×2 distributed multi-user MIMO OFDM transmission using real-time sigma-delta modulated signal over fiber (SDoF) links targeting 5G next generation fronthaul interface (NGFI) downlink. The OFDM baseband signals are sigma-delta modulated and digitally up-converted to a carrier frequency around 3.5 GHz on an FPGA; the signals are transmitted over OM4 multi-mode fibers using a commercial QSFP module at 850 nm.

The performance of the SDoF link satisfies the 3GPP error vector magnitude (EVM) requirements for 256-QAM (3.5%): the EVM of 163.84 MHz-bandwidth OFDM signals over 100 m OM4 multi-mode fibers is 3.14% (-30.06 dB). It is worth mentioning that the same hardware implementation is used for different bandwidths, proving the SDoF link is highly scalable to accommodate wide-bandwidth signals. Combining the SDoF links and MIMO transmission guarantees the frequency synchronism among remote radio units; as shown by the 2×2 MIMO performance, the wireless spectral efficiency almost doubles. An average EVM of 3.5% is measured for 40.96 MHz-bandwidth signals (64-QAM, 330 Mbps) and 6.66% for 163.84 MHz-bandwidth (64-QAM, 1.4 Gbps).

This work proves that combining SDoF and MIMO techniques is definitely a feasible and cost-efficient solution to meet the 5G challenges. Our future work includes extending the MIMO system to massive MIMO and implementing the setup for the 5G frequency range 2 (frequency band beyond 24 GHz).

Appendix

Singular Values of Channel Matrix H

To analyze the correlation between channel frequency responses (CFRs), we apply singular value decomposition (SVD) to the channel matrices $\mathbf{H}$. As described in (1), for one subcarrier, $\mathbf{H}$ is a 2×2 matrix.

$$\mathbf{H} = \begin{bmatrix} H_{11} & H_{21} \\ H_{12} & H_{22} \end{bmatrix} \tag{A.1}$$

where H_{ij} denotes the equivalent CFR in baseband between RRU i and receiver j. The SVD of $\mathbf{H}$ is

$$\mathbf{H} = \mathbf{U}\mathbf{S}\mathbf{V}^H \tag{A.2}$$

where the columns of $\mathbf{U}$ and $\mathbf{V}$ are formed by the left and right singular vectors of $\mathbf{H}$ respectively, $\mathbf{V}^H$ denotes the Hermitian transpose (conjugate transpose) of $\mathbf{V}$, and $\mathbf{S}$ is a diagonal matrix with non-negative real numbers on the diagonal. $\mathbf{S}$ contains the singular values, σ_1 and σ_2, of $\mathbf{H}$:

$$\mathbf{S} = \begin{bmatrix} \sigma_1 & 0 \\ 0 & \sigma_2 \end{bmatrix} \tag{A.3}$$

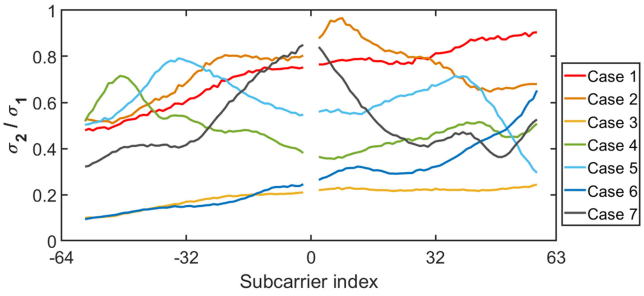

(a) 40.96 MHz

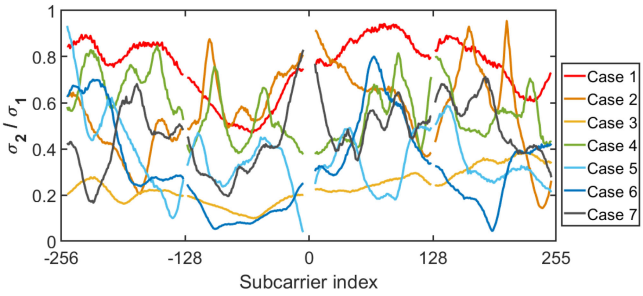

(b) 163.84 MHz

Fig. 10. Ratio of singular values (σ_2/σ_1) of the channel matrices ($\mathbf{H}$).

TABLE II
Average σ_2/σ_1 Over Non-Zero Subcarriers

Bandwidth	Case						
(MHz)	1	2	3	4	5	6	7
40.96	0.72	0.73	0.19	0.49	0.61	0.27	0.52
163.84	0.76	0.57	0.24	0.57	0.36	0.33	0.46

For MIMO channels that are highly correlated, the ratio of the two singular values, σ_2/σ_1, is close to zero, implying that both row vectors of $\mathbf{H}$, $[H_{11}H_{21}]$ and $[H_{12}H_{22}]$, are so similar that they can both be expressed as scalar products of one vector—the first column of $\mathbf{V}$. On the contrary, for MIMO channels that are totally independent, i.e. $\mathbf{H}$ is an identity matrix, σ_2/σ_1 is one.

Fig. 10 plots the ratios σ_2/σ_1 of all non-zero subcarriers for 40.96 MHz-bandwidth (Fig. 10a) and 163.84 MHz (Fig. 10b). Table II lists the average σ_2/σ_1 over non-zero subcarriers for each case (Fig. 7).

The ratios σ_2/σ_1 indicate the richness of the multipaths in the measurement environment. However, a small σ_2/σ_1 does not always result in a large MIMO-SISO performance difference, e.g. case 3. Case 3 has the smallest average σ_2/σ_1 for both the 40.96 MHz and 163.84 MHz case, but the MIMO-SISO performance difference is 0.47 dB for 40.96 MHz and 0.57 dB for 163.84 MHz. The accuracy of the estimated CFRs and the power difference between the signal and interference paths are more dominant factors as discussed in Subsection III-B.

REFERENCES

[1] A. Gupta and R. K. Jha, "A survey of 5G network: Architecture and emerging technologies," *IEEE Access*, vol. 3, pp. 1206–1232, 2015.

[2] C. I, H. Li, J. Korhonen, J. Huang, and L. Han, "RAN revolution with NGFI (xhaul) for 5G," *J. Lightw. Technol.*, vol. 36, no. 2, pp. 541–550, Jan. 2018.

[3] R. Irmer *et al.*, "Coordinated multipoint: Concepts, performance, and field trial results," *IEEE Commun. Mag.*, vol. 49, no. 2, pp. 102–111, Feb. 2011.

[4] T. Pfeiffer, "Next generation mobile fronthaul and midhaul architectures," *IEEE J. Opt. Commun. Netw.*, vol. 7, no. 11, pp. B38–B45, Nov. 2015.

[5] China Mobile Research Institute, "White paper of next generation fronthaul interface," 2015.

[6] "Study on new radio access technology: Radio access architecture and interfaces (release 14) (V14.0.0)," 3GPP, Sophia Antipolis Cedex, France, TR 38.801, 2017.

[7] C. Ranaweera, E. Wong, A. Nirmalathas, C. Jayasundara, and C. Lim, "5G C-RAN with optical fronthaul: An analysis from a deployment perspective," *J. Lightw. Technol.*, vol. 36, no. 11, pp. 2059–2068, Jun. 2018.

[8] "Common public radio interface (CPRI) specification V7.0," Oct. 2015. [Online]. Available: http://www.cpri.info/spec.html

[9] "Common public radio interface: eCPRI interface specification V2.0," May 2019. [Online]. Available: http://www.cpri.info/spec.html

[10] J. Wang, Z. Jia, L. A. Campos, and C. Knittle, "Delta-sigma modulation for next generation fronthaul interface," *J. Lightw. Technol.*, vol. 37, no. 12, pp. 2838–2850, Jun. 2019.

[11] A. Frappé, A. Flament, B. Stefanelli, A. Kaiser, and A. Cathelin, "An all-digital RF signal generator using high-speed $\Delta\Sigma$ modulators," *IEEE J. Solid-State Circuits*, vol. 44, no. 10, pp. 2722–2732, Oct. 2009.

[12] L. Breyne, G. Torfs, X. Yin, P. Demeester, and J. Bauwelinck, "Comparison between analog radio-over-fiber and sigma delta modulated radio-over-fiber," *IEEE Photon. Technol. Lett.*, vol. 29, no. 21, pp. 1808–1811, Nov. 2017.

[13] G. Torfs *et al.*, "ATTO: Wireless networking at fiber speed," *J. Lightw. Technol.*, vol. 36, no. 8, pp. 1468–1477, Apr. 2018.

[14] C.-Y. Wu *et al.*, "Real-time 4×3.5 Gbps sigma delta radio-over-fiber for a low-cost 5G C-RAN downlink," in *Proc. Eur. Conf. Opt. Commun.*, Rome, Italy, Sep. 2018, Paper Tu3B.1.

[15] H. Li *et al.*, "Real-time 100-GS/s sigma-delta all-digital radio-over-fiber transmitter for 22.75–27.5 GHz band," in *Proc. Opt. Fiber Commun. Conf.*, San Diego, CA, USA, Mar. 2019, Paper Th1F.4.

[16] S. Jayaprakasam, S. K. A. Rahim, and C. Y. Leow, "Distributed and collaborative beamforming in wireless sensor networks: Classifications, trends, and research directions," *IEEE Commun. Surv. Tut.*, vol. 19, no. 4, pp. 2092–2116, Oct.–Dec. 2017.

[17] A. E. Aighobahi and N. J. Gomes, "Capacity and error performance verification of multi-antenna schemes in radio-over-fiber distributed antenna system," *J. Lightw. Technol.*, vol. 34, no. 20, pp. 4779–4785, Oct. 2016.

[18] L. Cheng *et al.*, "Coordinated multipoint transmissions in millimeter-wave radio-over-fiber systems," *J. Lightw. Technol.*, vol. 34, no. 2, pp. 653–660, Jan. 2016.

[19] U. Habib, A. E. Aighobahi, T. Quinlan, S. D. Walker, and N. J. Gomes, "Analog radio-over-fiber supported increased RAU spacing for 60 GHz distributed MIMO employing spatial diversity and multiplexing," *J. Lightw. Technol.*, vol. 36, no. 19, pp. 4354–4360, Oct. 2018.

[20] I. C. Sezgin *et al.*, "A low-complexity distributed-MIMO testbed based on high-speed sigma–delta-over-fiber," *IEEE Trans. Microw. Theory Techn.*, vol. 67, no. 7, pp. 2861–2872, Jul. 2019.

[21] D. Jiang and G. Liu, "An overview of 5G requirements," in *Proc. 5G Mobile Commun.*, 2017, pp. 3–26.

[22] C.-Y. Wu *et al.*, "Distributed MU-MIMO demonstration using FPGA-based sigma-delta-over-fiber," in *Proc. Eur. Conf. Opt. Commun.*, Dublin, Ireland, Sep. 2019.

[23] A. Lozano and N. Jindal, "Transmit diversity vs. spatial multiplexing in modern MIMO systems," *IEEE Trans. Wireless Commun.*, vol. 9, no. 1, pp. 186–197, Jan. 2010.

[24] IEEE 802, "IEEE 802.11ac-2013," 2013.

[25] J.-J. van de Beek *et al.*, "On channel estimation in OFDM systems," in *Proc. IEEE 45th Veh. Technol. Conf. Countdown Wireless Twenty-First Century*, Chicago, IL, USA, Jul. 1995, vol. 2, pp. 815–819.

[26] H. Li *et al.*, "A 21-GS/s single-bit second-order delta-sigma modulator for FPGAs," *IEEE Trans. Circuits Syst., II, Express Briefs*, vol. 66, no. 3, pp. 482–486, Mar. 2019.

[27] J. Van Kerrebrouck *et al.*, "Real-time all-digital radio-over-fiber LTE transmission," in *Proc. Advances Wireless Opt. Commun.*, Riga, Latvia, Nov. 2017, pp. 83–86.

[28] O. Caytan *et al.*, "Passive opto-antenna as downlink remote antenna unit for radio frequency over fiber," *J. Lightw. Technol.*, vol. 36, no. 19, pp. 4445–4459, Oct. 2018.

[29] A. N. Mody and G. L. Stüber, "Synchronization for MIMO OFDM systems," in *Proc. GLOBECOM*, San Antonio, TX, USA, Nov. 2001, vol. 1, pp. 509–513.

[30] J. Li *et al.*, "Performance evaluation of cloud-RAN system with carrier frequency offset," in *Proc. GLOBECOM Workshops*, Anaheim, CA, USA, Dec. 2012, pp. 222–226.

[31] "Evolved universal terrestrial radio access (E-UTRA): Base station (BS) radio transmission and reception (release 16) (V16.2.0)," 3GPP, Sophia Antipolis Cedex, France, TS 36.104, Jul. 2019.

[32] "New radio (NR): Base station (BS) radio transmission and reception (release 16) (V16.0.0)," 3GPP, Sophia Antipolis Cedex, France, TS 38.104, Jun. 2019.

[33] Y. Yang *et al.*, "A low-complexity transceiver structure with multiple CFOs compensation for OFDM-based coordinated multi-point systems," *IEEE Trans. Commum.*, vol. 63, no. 7, pp. 2658–2670, Jul. 2015.

[34] J. J. van de Beek, M. Sandell, and P. O. Borjesson, "ML estimation of time and frequency offset in OFDM systems," *IEEE Trans. Signal Process.*, vol. 45, no. 7, pp. 1800–1805, Jul. 1997.

[35] A. Pizzinat, P. Chanclou, F. Saliou, and T. Diallo, "Things you should know about fronthaul," *J. Lightw. Technol.*, vol. 33, no. 5, pp. 1077–1083, Mar. 2015.